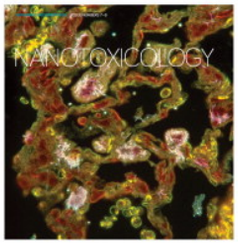

Nanotoxicology

ISSN: 1743-5390 (Print) 1743-5404 (Online) Journal homepage: www.tandfonline.com/journals/inan20

Lipidomics analysis reveals signature inflammatory and specialized pro-resolving mediators at the junction of inflammation-resolution transition in mouse lungs exposed to multiwalled carbon nanotubes

Qiang Ma, Chol Seung Lim, Ryan F. LeBouf, Chengetayi Cornelius Rimayi & Ju-Hyeong Park

To cite this article: Qiang Ma, Chol Seung Lim, Ryan F. LeBouf, Chengetayi Cornelius Rimayi & Ju-Hyeong Park (08 Jan 2026): Lipidomics analysis reveals signature inflammatory and specialized pro-resolving mediators at the junction of inflammation-resolution transition in mouse lungs exposed to multiwalled carbon nanotubes, Nanotoxicology, DOI: 10.1080/17435390.2025.2610342

To link to this article: https://doi.org/10.1080/17435390.2025.2610342

NANOTOXICOLOGY
https://doi.org/10.1080/17435390.2025.2610342

Taylor & Francis
Taylor & Francis Group

RESEARCH ARTICLE

Lipidomics analysis reveals signature inflammatory and specialized pro-resolving mediators at the junction of inflammation-resolution transition in mouse lungs exposed to multiwalled carbon nanotubes

Qiang Ma[a], Chol Seung Lim[a], Ryan F. LeBouf[b], Chengetayi Cornelius Rimayi[b] and Ju-Hyeong Park[b]

[a]Receptor Biology Laboratory, Toxicology and Molecular Biology Branch, Health Effects Laboratory Division, National Institute for Occupational Safety and Health, Centers for Disease Control and Prevention, Morgantown, WV, USA; [b]Field Studies Branch, Respiratory Health Division, National Institute for Occupational Safety and Health, Centers for Disease Control and Prevention, Morgantown, WV, USA

ABSTRACT

Pulmonary exposure to certain multiwalled carbon nanotubes (MWCNTs) triggers significant inflammation that is regulated temporally by powerful mediators of inflammation and resolution. Among these mediators, inflammatory lipid mediators (ILMs) and specialized pro-resolving mediators (SPMs) have garnered increasing attention. In this study, lipidomics analysis revealed that fibrogenic MWCNTs stimulate the production of signature ILMs and SPMs in mouse lungs, marking a phenotypic shift from acute inflammation to resolution. Mice exposed to 40 µg MWCNTs via oropharyngeal aspiration exhibited dynamic, polarized pulmonary inflammation. By day 7 post-exposure, lung tissue showed elevated M2 macrophage markers and cytokines, with lesions characterized by moderate neutrophil infiltration and a marked increase in macrophages within alveolar sacs and interstitial spaces. These macrophages contained engulfed nanoparticles and formed clusters of varying sizes. In vitro, MWCNTs promoted nanoparticle phagocytosis and cytoplasmic phospholipid accumulation. Lipidomics profiling of lung bioactive lipids, performed using ultraperformance liquid chromatography-tandem mass spectrometry, showed significant increases in ILMs and SPMs. These included prostaglandin (PG) E2, PGD2, thromboxane B2, leukotriene B4, and lipoxin B4 from the arachidonic acid pathway; resolvin (Rv) D5, protectin DX, maresin 1, 17-hydroxydocosahexaenoic acid (HDHA), and 14S-HDHA from the docosahexaenoic acid pathway; and RvE2, 15-hydroxyeicosapentaenoic acid (HEPE), and 18-HEPE from the eicosapentaenoic acid pathway. These findings suggest that MWCNTs trigger a distinct lipid mediator signature at the junction of inflammation-resolution transition to promote the programmatic switch from acute inflammation to resolution, supporting continued particle clearance, inflammation resolution, and return to homeostasis in response to nanoparticle exposure.

ARTICLE HISTORY
Received 29 September 2025
Revised 5 December 2025
Accepted 22 December 2025

KEYWORDS
MWCNT; lipidomics; lung inflammation; resolution of inflammation; fibrosis

Introduction

Pulmonary inflammation is a common and often prominent acute response to inhaled particles and nanoparticles, provided that the dose is sufficient relative to the potency of the particles (Ma 2020). While acute inflammation facilitates the clearance of inhaled particles, it can also cause damage to lung tissue due to the release of potent, cell-killing molecules from neutrophils and macrophages. Timely resolution of inflammation is crucial for recovery and the maintenance of tissue structure and function following exposure to a stimulus (Serhan and Savill 2005).

The initiation and resolution of inflammation are regulated by potent lipid mediators (LMs), which can either augment inflammation or promote the resolution of inflammation (Ricciotti and FitzGerald 2011, Chiang and Serhan 2020). Failure of resolution of inflammation leads to chronicity and adverse disease outcomes. In this connection, inflammatory lipid mediators (ILMs) recruit leukocytes and activate neutrophils and macrophages, both of which are critical for initiating and amplifying acute inflammation. ILMs include prostaglandins (PGs), thromboxane (TX), and leukotrienes (LTs), all derived from arachidonic acid (AA) through the cyclooxygenase (COX) and arachidonate 5-lipoxygenase (Alox5) pathways. On

CONTACT Qiang Ma qam1@cdc.gov Toxicology and Molecular Biology Branch, Health Effects Laboratory Division, National Institute for Occupational Safety and Health, Centers for Disease Control and Prevention, 1000 Frederick Lane, Morgantown, WV 26508, USA

the other hand, specialized pro-resolving mediators (SPMs) are produced to actively halt inflammation and promote tissue regeneration (Chiang and Serhan 2020). SPMs include lipoxins (LXs) generated from AA, D-series resolvins (RvDs), protectins, and maresins (MaRs) derived from docosahexaenoic acid (DHA), as well as E-series resolvins (RvEs) from eicosapentaenoic acid (EPA). While AA is a ω-6 polyunsaturated fatty acid (PUFA) synthesized de novo in the human body, DHA and EPA are ω-3 PUFAs primarily obtained from dietary sources.

Multiwalled carbon nanotubes (MWCNTs) are carbon allotropes composed of multiple concentric cylindrical layers formed by graphene-like sheets. These sheets consist of carbon atoms arranged in hexagonal lattices through sp^2 hybridization (Sinnott and Andrews 2001). MWCNTs possess excellent tensile strength, electrical conductivity, and thermal and optical properties, making them of particular interest for various industrial and commercial applications (De Volder et al. 2013, Zhang et al. 2013, Hughes et al. 2024). However, due to their airborne nature and resistance to degradation, there are concerns regarding potential long-lasting health effects when inhaled by workers and consumers (Donaldson et al. 2006, NIOSH. 2013, Dong and Ma 2019). Toxicological studies in laboratory animals have shown that certain MWCNTs can induce lung inflammation and other lesions with potencies comparable to those of respirable mineral particles and fibers known to cause lung fibrosis and cancer in humans, such as silica and asbestos (Porter et al. 2010, Mercer et al. 2013, Dong and Ma 2015, Dong et al. 2015, Suzui et al. 2016).

MWCNT-induced lung inflammation exhibits polarized, biphasic responses (Dong and Ma 2018a, Ma 2020). The early phase is characterized by type 1 inflammation, marked by rapid neutrophil infiltration, high levels of proinflammatory cytokines, and phagocytosis of particles by classically activated (M1) macrophages (Porter et al. 2010, Dong et al. 2015). Neutrophil infiltration peaks at 1-day post-exposure, while M1 macrophage accumulation peaks at 3-days post-exposure. Following this initial response, neutrophils are rapidly cleared from inflammatory sites, and macrophages continue to accumulate, adopting the phenotypes of alternatively activated (M2) macrophages, which are key mediators of type 2 inflammation. This type 2 inflammation is characterized by the resolution of inflammation and fibroproliferation, leading either to tissue repair and recovery or to chronic outcomes such as fibrosis (Dong and Ma 2016, Dong and Ma 2018b, Lim et al. 2020).

The time-dependent polarization of lung macrophages into M1 and M2 states is critical for the regulation of particle- and nanoparticle-induced lung inflammation through ILMs and SPMs. In this context, the phagocytosis of particles activates the COX- and Alox5-dependent pathways to produce inflammatory prostanoids and leukotrienes in M1 macrophages (Lim et al. 2020, Lim et al. 2023, Lim, Gu, and Ma 2025), whereas tissue damage caused by particle depositition and inflammation over time stimulates the synthesis and secretion of SPMs from DHA, EPA, and AA through Alox5- and Alox15-dependent pathways to mediate resolution of lung inflammation (Lim et al. 2020).

The significant role of ILMs and SPMs in inflammation and its resolution has generated considerable interest in understanding their functions and regulation during the temporal evolution and outcomes of lung inflammation induced by particles and nanoparticles. Fibrogenic MWCNTs have been shown to stimulate the production of ILMs, such as PGE2 and LTB4, in mouse lungs and bronchoalveolar lavage fluid (BALF) during acute inflammation, as well as SPMs, such as LXs and RvDs, in later phases of inflammation (Lim et al. 2020). MWCNTs have also been found to induce the expression of the Cox-2 enzyme in allergen and MWCNT-stimulated airway remodeling in mice (Sayers et al. 2013). Given the complexity of the networks formed by ILMs and SPMs, we recently developed a method using ultraperformance liquid chromatography-tandem mass spectrometry (UPLC-MS/MS) that, when combined with a C18 spin column solid phase extraction, enabled efficient lipidomics profiling of LMs in mouse lungs during acute inflammation induced by fibrogenic MWCNTs (Ma et al. 2025).

Considering the polarized and biphasic nature of MWCNT-induced lung inflammation, we hypothesize that MWCNTs stimulate the synthesis of SPMs during the transition from neutrophil-predominant type 1 inflammation to macrophage-predominant type 2 inflammation, thereby promoting the resolution of inflammation. In this study, we performed lipidomics profiling of ILMs and SPMs at 7 days post-exposure to MWCNTs, a time point at which acute inflammation is expected to transition to resolution or chronic progression (Dong and Ma 2016, 2018b). Our findings indicate that MWCNTs induced macrophage-predominant inflammation in mouse lungs during the transition. We observed that MWCNTs stimulated the phagocytosis of particles by macrophages and the accumulation of phospholipids in the cytoplasm *in vitro*. Lipidomics profiling revealed that MWCNTs increased the production of ILMs, including PGH2, PGE2, PGD2, TXB2, and LTB4, as well as SPMs, including LXB4, RvD5, RvE4, MaR1, and PDX, a signature of LMs that facilitate the continued clearance of particles and the resolution of

sterile inflammation in mouse lungs exposed to fibrogenic MWCNTs.

Materials and methods

MWCNTs and preparation

MWCNTs used in this study were sourced from Mitsui & Company (Mitsui-7, XNRI 1, lot #05072001K28, Tokyo, Japan). MWCNTs were imaged using transmission electron microscopy (TEM), as described in our previous publication (Lim et al. 2023). Stock samples prepared as described below were further diluted in double distilled H_2O to 1:300 for most of the samples. One drop of the diluted samples was placed onto a formvar-coated 200 mesh copper grid and allowed to dry overnight. The samples were imaged using a JEOL 1400 TEM (Tokyo, Japan) at 80 kV. For MWCNTs, length measurements were taken from the longest straight distance between two points. The width measurement was the distance perpendicular to the structural walls of the CNTs.

The MWCNTs have a log-normal length distribution with a mean length of 4.46 µm (95% confidence interval: 4.08–4.88 µm) and a normal width distribution with a mean of 58.5 nm (95% confidence interval: 56.0–61.0 nm). The MWCNTs are rod-like fibers (Figure 1(A)) with a surface area of 26 m^2/g, containing low levels of trace elements (0.78% for all metals and 0.32% for iron) (Porter et al. 2010). The level of lipopolysaccharides in the MWCNTs was determined to be <0.01 mg/mL or <0.1 EU/mL using the Pierce LAL chromogenic endotoxin quantification kit (Thermo Fisher Scientific, Pittsburgh, PA).

For animal treatment, MWCNTs were prepared as described previously (Porter et al. 2010, Lim et al. 2020). The dispersion medium (DM) consisted of 0.9% saline, 0.6 mg/mL mouse serum albumin (Millipore Sigma, Burlington, MA, USA), and 0.01 mg/mL 1,2-dipalmitoyl-sn-glycero-3-phosphocholine (Millipore Sigma). MWCNTs were suspended in DM following a two-step dispersion procedure involving sonication. DM was also used as the vehicle control for MWCNTs in animal experiments. For cell culture treatment, MWCNTs were suspended in Dulbecco's Modified Eagle's Medium (DMEM, Thermo Fisher Scientific) containing 1% fetal bovine serum (FBS, Thermo Fisher Scientific) using vortexing and sonication. The DMEM with 1% FBS served as the vehicle control for MWCNTs in cell culture.

Animals and treatment

Adult male C57BL/6J mice were obtained from the Jackson Laboratories (Bar Harbor, ME, USA) and housed in an accredited, specific pathogen-free, and environmentally controlled facility at the National Institute for Occupational Safety and Health. The mice were kept in polycarbonate ventilated cages with HEPA-filtered air and maintained on a 12-hour fluorescent lighting schedule. They were provided with Harlan Teklad Rodent Diet 7913 (Indianapolis, IN, USA) and tap water *ad libitum*. All animal experiments were conducted in accordance with humane care guidelines and were approved by the Institutional Animal Care and Use Committee.

Mice were treated with a single dose of MWCNTs (40 µg/mouse, adjusted to body weight) or vehicle control (dispersion medium, DM, 50 µL/mouse, adjusted to body weight) via oropharyngeal aspiration. Euthanasia was performed using an intraperitoneal injection of a sodium pentobarbital euthanasia solution (100–300 mg/kg body weight; Zoetis, Florham Park, NJ, USA), followed by exsanguination once the mouse became unresponsive to toe pinch.

Oropharyngeal aspiration is a noninvasive route of administration to deliver a specific dose of respirable materials, such as nanoparticles, into animal lungs to result in an even distribution of the materials in the lungs (Rao et al. 2003). MWCNTs at 40 µg in 50 µL administered by aspiration induced rapid and pronounced acute inflammation in mouse lungs, characterized by significant neutrophil infiltration and the secretion of proinflammatory cytokines (Porter et al. 2010, Dong et al. 2015, Lim et al. 2020). At nearly equivalent lung burdens of the MWCNTs, lung inflammation on day 1 post-exposure was similar between a single dose exposure by aspiration at a dose of 80 µg/mouse and by aerosol inhalation at 5 mg/m^3, 5 hours/day, 12 days (Mercer et al. 2013). This inhalation paradigm results in a lung burden in mice equal to a predicted human lung burden on an equivalent alveolar surface area basis for a person performing light work at 7 µg/m^3 for 13 years. These MWCNTs at 40 or 80 µg were shown to produce comparable pulmonary effects (Porter et al. 2010). Thus, a dose of the MWCNTs at 40 or 80 µg by aspiration in mice would produce an initial lung burden in humans comparable to that by inhalation.

There has been a paucity of data on human exposure to engineered nano materials. It has been estimated that this dose of 40 µg MWCNT exposure in mice approximates human deposition for a person performing light work for 11 years (Lim et al. 2020). This estimation assumes that a worker performs light work in an environment with MWCNT aerosol of

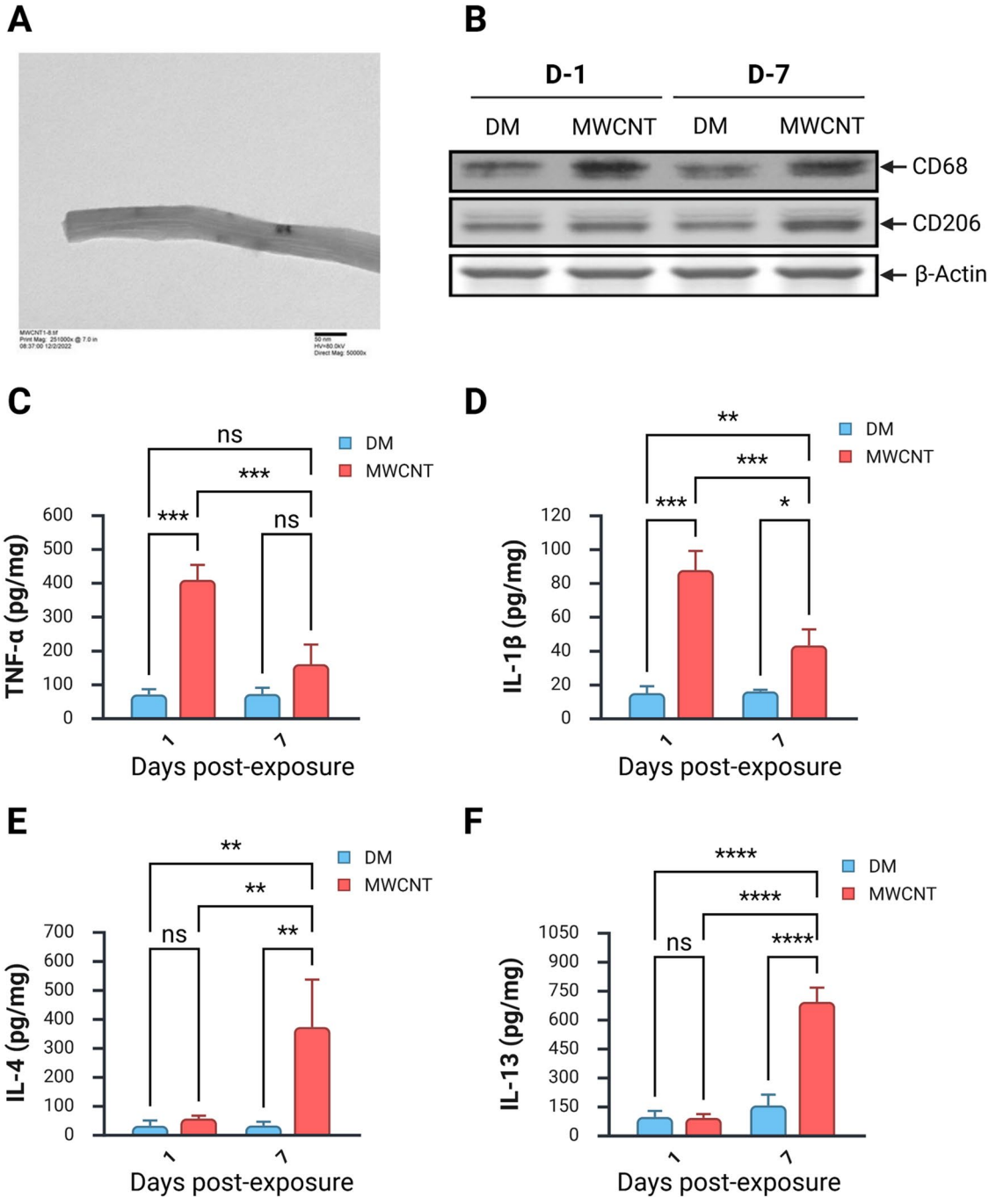

Figure 1. MWCNT-induced polarization of inflammation in mouse lungs. Adult male C57BL/6J mice were exposed to either vehicle (DM) or MWCNTs (40 µg/mouse adjusted to body weight) via oropharyngeal aspiration. Lung tissue was collected at 1-day and 7-days post-exposure. (A) EM imaging of MWCNTs. The Mitsui-7 MWCNTs are rod-like fibers under TEM at 50,000x magnification. (B) Immunoblotting of M1 (CD68) and M2 (CD206) markers. β-actin was blotted as loading control. (C)-(F) Lung type 1 (TNF-α and IL-1β) and type 2 (IL-4 and IL-13) cytokines quantified by ELISA. Data represents mean ± SD from 3 mice each group. Statistical significance is indicated as ns (non-significance), *$p < 0.05$, **$p < 0.01$, ***$p < 0.001$, ****$p < 0.0001$.

10.6 mg/m^3 (Erdely et al. 2013) and has a minute ventilation of 20 L/min (Galer et al. 1992), a deposition faction of 30% (Phalen 2008), and an alveolar epithelium surface area of 102 m^2 (Stone et al. 1992), which gives an estimated human exposure per year of 7.3 mg/m^2 alveolar epithelium.

Animal lung collection, histology, and immunohistochemistry

After euthanasia, mouse lungs were collected from four mice each group for analysis. The right lung lobes were minced, frozen in liquid nitrogen, and stored at

−80 °C for lipidomics and protein analyses. The left lungs were formalin-fixed, paraffin-embedded, and sectioned to 5 microns. Lung sections were stained using hematoxylin-eosin (H&E) staining or Masson's trichrome staining (MTS) following standard procedures.

For immunohistochemistry, lung sections were deparaffinized with three washes of xylene (5 minutes each), rehydrated with two washes of 100% ethanol (10 minutes each), two washes of 95% ethanol (10 minutes each), and one wash of 70% ethanol (5 minutes), followed by two washes with deionized water (5 minutes each). To unmask antigens, sections were heated in a 10 mM sodium citrate buffer (pH 6.0) at sub-boiling temperature (10 minutes) in a microwave oven, followed by cooling on a benchtop for 30 minutes. The slides were then incubated with a BLOXALL endogenous peroxidase and alkaline phosphatase blocking solution (Vector Laboratories, Burlingame, CA, USA) for 10 minutes. Immunohistochemistry was performed using the ImmPRESS polymer detection system (Vector Laboratories) with ImmPACT NovaRED as a peroxidase substrate (red in color). Nuclei were counterstained with hematoxylin OS (blue violet in color, Vector Laboratories). Primary antibodies used included anti-Mac2 for macrophage detection (Cedarlane, Burlington, Ontario, Canada) and anti-neutrophil for neutrophil detection (Abcam, Cambridge, MA, USA). Images were captured using an Olympus Provis AX-70 microscope (Olympus, Center Valley, PA, USA). Positively stained cells were counted from five images taken at 40x magnification from one section, and lung sections from four mice in each group were examined.

Cell culture and detection of phospholipids

J774A.1 murine monocyte/macrophage cell line was obtained from the American Type Culture Collection (ATCC, Manassas, VA, USA). Cells were cultured in DMEM with 10% FBS in a cell culture incubator at 37 °C with 5% CO_2. J774A.1 cells are known to avidly phagocytose nanoparticles and secrete significant amounts of proinflammatory cytokines, such as interleukin (IL)-1β and tumor necrosis factor (TNF)-α, in response to nanoparticle exposure, mirroring the behavior of mouse alveolar macrophages (Lim et al. 2020, Lim et al. 2023, Lim, Gu, and Ma 2025).

Cells were plated on a 24-well plate overnight, followed by treatment with vehicle control or MWCNTs at a concentration of 2 µg/mL for 24 hours. At this dose, MWCNTs induce prominent proinflammatory responses in J774A.1 macrophage cells (Lim et al. 2020, Lim et al. 2023). After treatment, the cells were stained with the LipidTox Red Phospholipidosis reagent (LTRP, Thermo Fisher Scientific) for an additional 24 hours under the same culture conditions before fixation with 3.7% formaldehyde. The nuclei were counterstained using 4′,6-diamidino-2-phenylindole (DAPI, Thermo Fisher Scientific). Images were captured using the Agilent BioTek Cytation 1 Cell Imaging Multi-Mode Reader (Model CYT1FAV, Agilent, San Diego, CA, USA), utilizing phase contrast for optical morphology, a DAPI filter for DAPI fluorescence (EX 360 nm, EM 460 nm), and a TRITC filter for LTRP fluorescence (EX 595 nm, EM 615 nm). Scale bars were set at 200 µm. Images were analyzed for relative fluorescence intensity (RFU) using the Gen5 software (Agilent). Data were presented as mean ± SD from four separate cell populations.

UPLC–MS/MS chemicals

All chemicals used for UPLC–MS/MS analysis were of LCMS grade and obtained from Fisher Scientific (Pittsburgh, PA, USA). Methanol and acetonitrile were >99.9% pure, and acetic acid was 99.9% pure. Ultrapure water was prepared using a Millipore LC pak polisher cartridge with a Millipak Express Filter MPGP04001 (Millipore Sigma).

Lipidomics standards for LMs

A total of 36 target standards and five deuterium-labeled internal standards were utilized for the calibration and quantification of LMs, as described previously (Ma et al. 2025). The standards were sourced from Cayman Chemicals (Ann Arbor, MI, USA) and had purities of ≥98%. Each sample was spiked with 100 pg/mL of the internal standards. Calibration standards for the target LMs were prepared across two ranges to accommodate varying levels of endogenous LMs in samples. The linear calibration range was from 0.66 pg/µL to 675 pg/µL for most LMs, while EPA, AA, and DHA had a range of 0.82 pg/µL to 13,500 pg/µL. The limit of detection (LOD) and limit of quantitation (LOQ) were calculated at 3× and 10× the signal-to-noise ratio, respectively.

The 36 target standards included various hydroxyeicosatetraenoic acids (HETEs), resolvins, lipoxins (LXs), prostaglandins (PGs), protectins, and thromboxane (TX). The specific compounds analyzed were: 5-hydroxyeicosapentaenoic acid (5-HEPE), 5-hydroxyeicosatetraenoic acid (5-HETE), 12-hydroxyeicosapentaenoic acid (12-HEPE), 12-hydroxyeicosatetraenoic acid (12-HETE), 14S-hydroxyhexaenoic acid (14S-HDHA), 15-hydroxyeicosapentaenoic acid (15-HEPE), 15-hydroxyeicosatetraenoic acid (15-HETE),

15R-lipoxin A4 (15R-LXA4), 17-hydroxyhexaenoic acid (17-HDHA), 17R-resolvin D1 (17R-RvD1), 17R-resolvin D4 (17R-RvD4), 18-hydroxyeicosapentaenoic acid (18-HEPE), arachidonic acid (AA), docosahexaenoic acid (DHA), eicosapentaenoic acid (EPA), leukotriene B4 (LTB4), lipoxin A4 (LXA4), lipoxin A5 (LXA5), lipoxin B4 (LXB4), maresin 1 (MaR1), maresin 2 (MaR2), prostaglandin D2 (PGD2), prostaglandin E2 (PGE2), prostaglandin F2α (PGF2α), prostaglandin H2 (PGH2), protectin D1 (PD1), protectin DX (PDX), resolvin D1 (RvD1), resolvin D2 (RvD2), resolvin D3 (RvD3), resolvin D4 (RvD4), resolvin D5 (RvD5), resolvin E1 (RvE1), resolvin E2 (RvE2), resolvin E4 (RvE4), and thromboxane B2 (TXB2).

The five deuterium-labeled internal standards included: 5S-hydroxy-6E,8Z,11Z,14Z-eicosatetraenoic-5,6,8,9,11,12,14,15-d8 acid (5S-HETE-d8), 5S,12R-dihydroxy-6Z,8E,10E,14Z-eicosatetraenoic-6,7,14,15-d4 acid (LTB4-d4), 5S,6R,15S-trihydroxyicosa-7E,9E,11Z,13E-tetraenoic-19,19,20,20,20-d5 acid (LXA4-d5), 9-oxo-11α,15S-dihydroxy-prosta-5Z,13E-dien-1-oic-3,3,4,4-d4 acid (PGE2-d4), and 7S,16R,17S-trihydroxy-4Z,8E,10Z,12E,14E,19Z-21,21′,22,22,22-d5 docosahexaenoic acid (RvD2-d5).

Sample preparation for liquid chromatography

Mouse lung tissue samples (four mice each group) were homogenized in ice-cold methanol (375 µL, LCMS grade, Fisher Scientific) spiked with 25 µL of the internal standards mixture using a Dounce homogenizer. The homogenates were incubated at −20 °C for 30 minutes, followed by centrifugation at 751 × g for 10 minutes to obtain supernatants. The supernatants were then acidified to pH 3.5.

Solid phase extraction

Lipids were extracted using solid-phase extraction with a C18 spin column (BioPureSPN Midi PROTO 300 C18, 17–170 mg, P/N HEM S18V) obtained from the Nest Group (Ipswich, MA, USA). Briefly, sample extracts were evaporated under a gentle stream of nitrogen using a TurboVap (Zymark, Hopkinton, USA) and reconstituted in 250 µL of a Milli-Q water:methanol mixture (80:20, v/v) with vortexing for 15 seconds. The reconstituted sample was added to a pre-conditioned C18 spin column, followed by pulse-spin at up to 1500 × g to remove the flow-through. The C18 column was washed with two volumes of 250 µL Milli-Q water:methanol (80:20, v/v). Lipids were then eluted by adding 250 µL of acetonitrile:Milli-Q water (80:20, v/v) on top of the C18 sorbent, followed by pulse-spin centrifugation past 1500 × g. The eluent was collected in a 1.5 mL centrifuge tube and evaporated to dryness using the TurboVap under a gentle nitrogen stream at 47 °C. The dried eluent was reconstituted in 45 µL of a mobile phase solvent mixture (A: B, 1:1, v/v) for immediate LC-MS/MS analysis, along with freshly prepared calibration internal standards.

Ultraperformance liquid chromatography (UPLC)

A liquid chromatography-tandem quadrupole mass spectrometer (Waters ACQUITY Xevo TQ-XS UPLC-MS, Waters, Milford, MA, USA) was utilized for lipidomic analysis (Ma et al. 2025). The Acquity Premier UPLC system was operated with an ACQUITY Premier HSS T3 column (1.8 µm, 2.1 × 100 mm, Product number 186009471, Waters) using a 10 µL injection volume. The column and sample tray temperatures were maintained at 50 °C and 4 °C, respectively, throughout the chromatographic runs. The mobile phase gradient consisted of solvent A (95% Milli-Q ultrapure water, 5% methanol, and 0.01% acetic acid with 10 mM ammonium acetate) and solvent B (95% methanol, 5% Milli-Q ultrapure water, and 0.01% acetic acid with 10 mM ammonium acetate). The flow rate was set to 200 µL/min. The gradient began with 100% solvent A and 0% solvent B, gradually increasing solvent B to 70% over 17 minutes. Solvent B was then increased to 85% over three minutes (from 17 to 20 minutes) and to 100% at 25 minutes, where it was held for 2 minutes. For re-equilibration, solvent B was reduced to 0% from 27 to 28 minutes and held for an additional 2.5 minutes. The total running time for each cycle was 30.5 minutes.

Mass spectrometry parameters and transitions

The tandem quadrupole mass spectrometer (Waters Xevo TQ-XS) was operated with an electrospray ionization (ESI) source in negative-ionization mode for the analysis of target analytes. The instrument was set with an ESI capillary voltage of 1.5 kV, and the source and desolvation temperatures were maintained at 150 °C and 250 °C, respectively. High-purity nitrogen (Peak Scientific Instruments, Westford, MA, USA) was used with desolvation and cone gas flow rates of 600 and 150 L/hour, respectively. The collision cell entrance and exit potentials were both set to 30 V. The system operated in multiple reaction monitoring (MRM) mode, with 4 to 5 optimized transitions for each compound, except for 12-HEPE, which had 2 reliable transitions optimized and used. The cone voltage and collision energy were individually optimized for each compound as described for a previous study (Ma et al. 2025).

Immunoblotting

Lung tissues treated as indicated above were extracted in a lysis buffer (10 mM Tris, pH 7.4, 1% SDS) with a 1x proteinase inhibitor cocktail (Thermo Fisher Scientific) using a tissue homogenizer (Omni International, GA, USA) following sonication for 10 seconds. The supernatant was collected and combined for each treated group (3 samples/each treated group). Tissue proteins (20 µg each sample) were fractionated on a 8 or 10% SDS-PAGE gel and transferred onto a nitrocellulose membrane. The membrane was incubated with 5% nonfat dry milk in tris-buffered saline with 0.05% Tween 20 for 1 hour at room temperature to block nonspecific binding, before incubation with primary antibodies. The primary antibodies used were mouse anti-CD68 (1:200, Novus Biologicals, Centennial, CO, USA), mouse anti-CD206 (1:250, Abcam), or mouse anti-β-actin (1:4,000, Millipore Sigma) antibodies. After incubation with horseradish peroxidase-conjugated goat anti-mouse or goat anti-rabbit IgG (both from Jackson ImmunoResearch laboratories, West Grove, PA; 1:5,000), immunoreactive bands were developed with Enhanced chemiluminescence (Thermo Fisher Scientific) on X-ray films. Film images were scanned using HP scanjet (Hewlett-Packard, Palo Alto, CA, USA) and were used to quantify each band with ImageJ software (NIH) with normalization to β-actin level.

Enzyme-linked immunosorbent assay (ELISA)

Proinflammatory type 1 (IL-1β, TNF-α) or type 2 cytokines (IL-4, IL-13) were detected in lung tissue extracts collected from mouse lungs exposed to DM or MWCNTs for the indicated dose and days using ELISA (three mice each group). All ELISA kits were purchased from MyBioSource (San Diego, CA, USA) and measurement was performed by following the manufacturer's protocol using a microplate reader equipped with the GEN5 software (Agilent).

Statistical analysis

Statistical comparisons between two means were performed using Welch's t-test, which accounts for possible unequal variances. Comparisons of multiple means were perfomed using mixed-model one-way analyses of vairance (AVOVA), followed by posthoc comparisons between two means. For LC–MS/MS analysis, means ± SD obtained from the lungs of four animals in each group were calculated. For cell culture analysis, means ± SD from four separate cell populations were used. Statistical analysis was conducted using the BioRender software (Science Suite Inc. DBA BioRender, Toronto, Ontario, Canada). Significance was set at $p < 0.05$ and indicated as follows: ns (non-significance), $^{*}p < 0.05$; $^{**}p < 0.01$; $^{***}p < 0.001$; and $^{****}p < 0.0001$.

Result

MWCNTs induced inflammation-to-resolution transition at 7 days post-exposure in mouse lung

The Mitsui-7 MWCNTs administered at a single dose induced acute inflammation in mouse lungs that exhibited time-dependent polarization and resolution. Acute inflammation was most prominent at 1-day post-exposure, characterized by polarization of macrophages into M1 cells (Figure 1(B)) and production of high levels of proinflammatory cytokines TNF-α and IL-1β (Figures 1(C and D)), consistent with it being M1- and neutrophilic type 1 inflammation (Dong et al. 2015; Lim et al. 2020; Ma et al. 2025).

At 7-days post-exposure, lung inflammation was marked by polarization of macrophages into M2 cells (Figure 1(B)) and production of high levels of pro-resolving cytokines IL-4 and IL-13 (Figures 1(E and F)). Lung lesions at 7-days post-exposure were further examined by immunohistochemistry. In vehicle-exposed lungs, the alveolar structure was well-preserved, with a low but detectable level of neutrophils present in both alveolar sacs and septa (Figure 2(A)). MWCNTs significantly increased the cellularity in the lung, particularly in inflammatory foci where MWCNTs were visible as black deposits (Figure 2(B)). MWCNT exposure resulted in a doubling of neutrophil numbers, although this increase did not reach statistical significance (Figure 2(E)). In contrast, the number of macrophages in the alveolar sacs increased dramatically, with MWCNTs causing a 7.7-fold increase in macrophage numbers in both the alveolar sacs and interstitial space (Figures 2(C, D and F)). Many macrophages formed clusters and contained engulfed MWCNT particles.

These results indicate a phenotypic switch from type 1 to type 2 inflammation at 7-days post-exposure. In view of the critical role of type 2 responses in inflammation resolution and tissue repair, we posited that MWCNTs activate the production of SPMs to promote the resolution of inflammation at 7 days post-exposure where a transition from acute inflammation to fibrotic progression was suggested (Dong and Ma 2018b; Ma 2020).

MWCNTs stimulated phagocytosis and induced accumulation of phospholipids in macrophages in vitro

Given that a significant portion of macrophages in the lungs of MWCNT-exposed mice contained engulfed

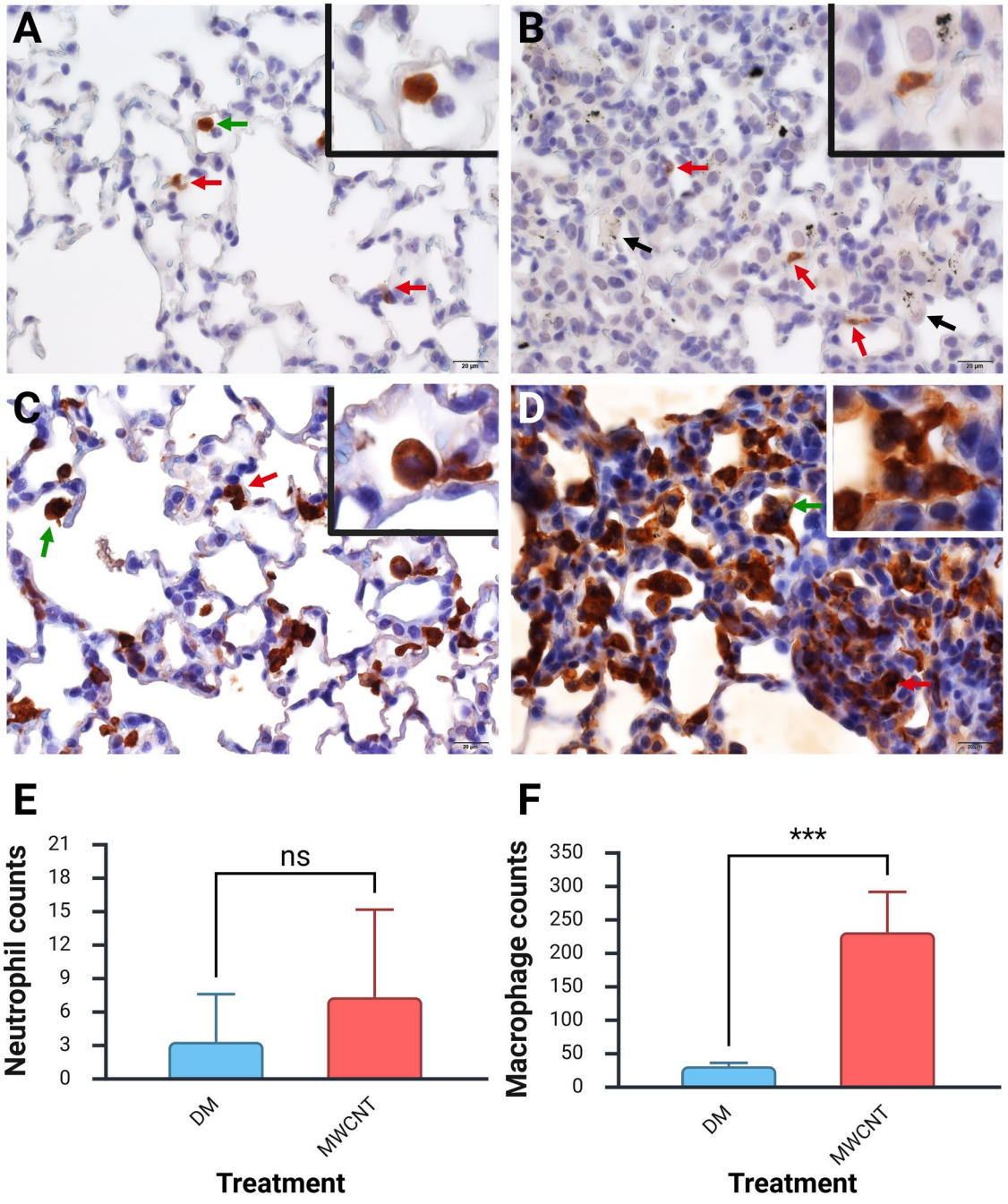

Figure 2. MWCNT-Induced inflammation-to-resolution transition in mouse lungs at 7-days post-exposure. Mice were treated as described in Figure 1. Lung tissue was collected at 7-days post-exposure. Lung sections were stained for neutrophils (A, B; anti-Ly-6G and Ly-6C, red) or macrophages (C, D; anti-Mac2, red) using immunohistochemistry. Red arrows indicate phagocytes in alveolar septa; green arrows indicate phagocytes in the alveolar cavity; and black arrows indicate macrophages containing engulfed MWCNTs. Quantification of neutrophil (E) and macrophage (F) accumulation is shown as mean ± SD from samples of four mice in each group. Statistical significance is indicated as ns (non-significance) and ***$p < 0.001$.

MWCNTs, we investigated the impact of MWCNT phagocytosis on the accumulation of phospholipids, which can serve as precursors for ILMs and SPMs in macrophages. J774A.1 murine macrophages were exposed to either vehicle control or MWCNTs at a concentration of 2 µg/mL for 24 hours. Following treatment, cells were stained with the LipidTox Red Phospholipidosis reagent (LTRP) to visualize intracellular phospholipids.

As shown in Figure 3, vehicle-exposed cells exhibited low levels of LTRP fluorescence, indicating minimal phospholipid accumulation (Figures 3(A–C)). In contrast, MWCNT-treated cells displayed a substantial increase in LTRP fluorescence, which did not overlap

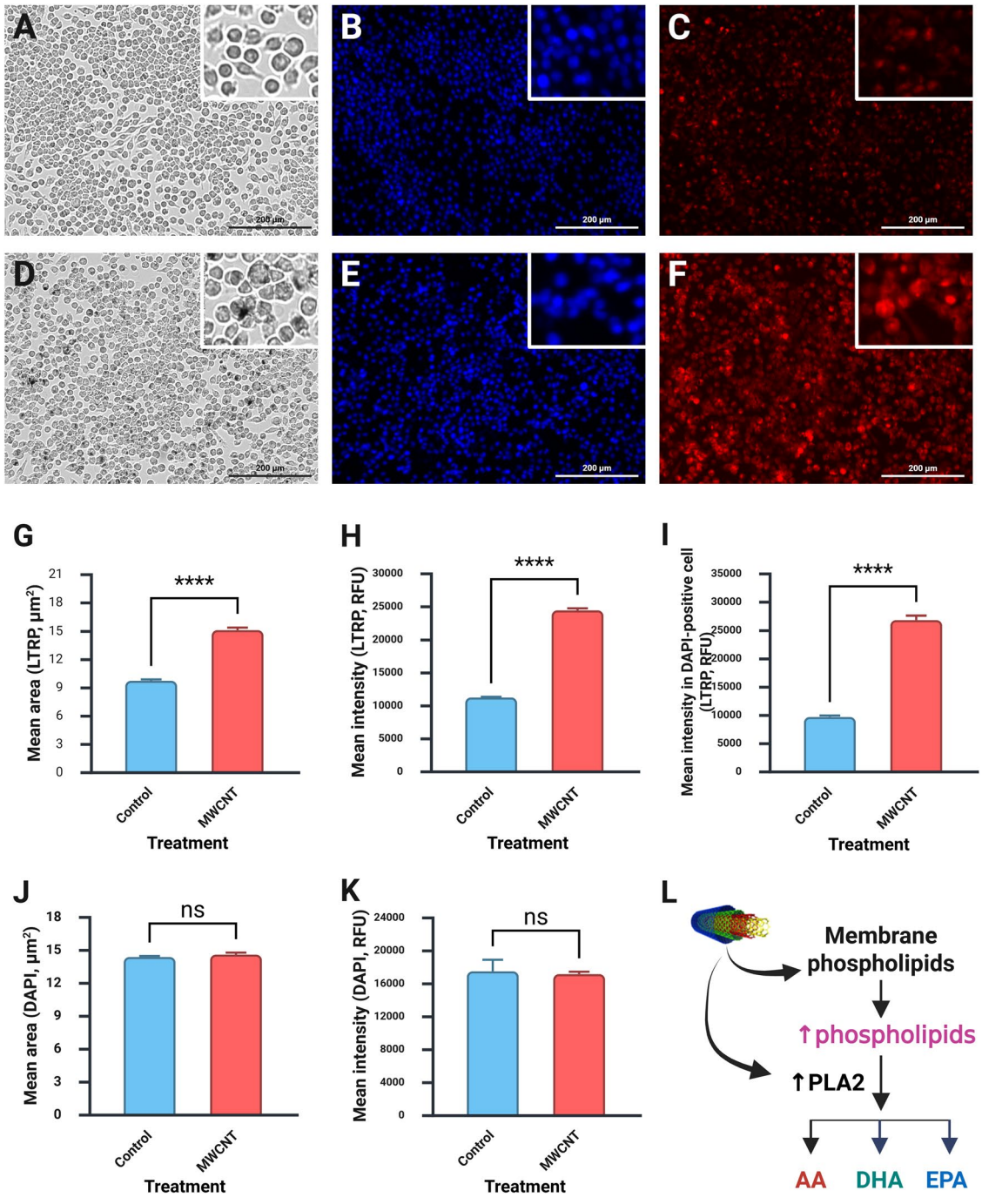

Figure 3. MWCNT-Induced accumulation of phospholipids in macrophages. J774A.1 macrophage cells were cultured in DMEM with 10% FBS overnight and then treated with either vehicle control (A-C) or MWCNTs at 2 µg/mL (D-F) for 24 hours. Following treatment, cells were stained with LTRP for an additional 24 hours and then fixed with 3.7% formaldehyde. DAPI was used to counterstain the nuclei. Images were captured using phase contrast for cell morphology (A, D), a DAPI filter for DAPI fluorescence (B, E), and a TRITC filter for LTRP fluorescence (C, F). Scale bar was set at 200 µm. Quantification of fluorescence intensity is shown in (G)-(K). (L) Illustration of the pathway through which MWCNTs increased phospholipid levels in macrophages, leading to the release of polyunsaturated fatty acids such as AA, DHA, and EPA. Data represent mean ± SD from four separate samples. Statistical significance is indicated as ns (non-significance) and ****$p < 0.0001$. RFU: relative fluorescence unit. PLA2, phospholipase A2.

with DAPI fluorescence, suggesting significant accumulation of phospholipids in the cytoplasm (Figures 3(D–F)). Quantitative analysis revealed increases in mean area per cell, mean intensity per cell, and mean intensity per DAPI-positive cell in MWCNT-exposed macrophages, all with statistical significance (Figures 3(G–I)). The DAPI fluorescence levels remained comparable between vehicle- and MWCNT-exposed cells (Figures 3(J–K)). These findings support the notion that MWCNTs stimulate the release of phospholipids from

membranes in macrophages, potentially serving as precursors for the synthesis of lipid mediators.

COX-dependent production of PGs and TXs from AA

To identify and quantify ILMs and SPMs, we performed targeted lipidomics analysis of 36 LMs using UPLC–MS/MS. The analysis revealed that MWCNTs significantly elevated the levels of several inflammatory lipid mediators at 7-days post-exposure. As illustrated in Figure 4(A), the major pathways involved in the production of ILMs from arachidonic acid via COX-dependent synthesis were activated. At this time point, AA levels were detected in both vehicle- and MWCNT-exposed lungs without a significant difference (Figure 4(B)). However, the levels of three major prostaglandins—PGH2, PGE2, and PGD2—were significantly increased in MWCNT-exposed lungs compared to vehicle controls (Figures 4(C–E)). Additionally, thromboxane B2 (TXB2), a major TX, was also significantly elevated by MWCNT exposure (Figure 4(F)). Prostaglandin F2α (PGF2α) was detected in vehicle-treated lungs and showed an increase in MWCNT-exposed lungs, although this increase did not reach statistical significance (Figure 4(G)).

ALOX-dependent production of LTs and LXs from AA

The analysis of leukotrienes and lipoxins produced from arachidonic acid via the Alox-mediated pathway revealed significant findings. As shown in Figure 5(A), LTs and LXs are formed from AA via separate Alox pathways. MWCNTs significantly elevated the levels of LTB4, a major chemoattractant for leukocytes, compared to control, indicating its critical role in the recruitment of polymorphonuclear leukocytes during inflammation (Figure 5(B)). Additionally, 5-HETE, which is produced from the same precursor as LTB4, was detected in vehicle-exposed lungs and showed an increase in MWCNT-exposed lungs, although this increase did not reach a statistical significance (Figure 5(C)).

Conversely, LXB4, a major SPM that inhibits leukocyte recruitment, is produced via Alox15. LXB4 was detected at high levels in vehicle-exposed lungs and was significantly elevated by MWCNT exposure, showing a 9.3-fold increase (Figure 5(D)). Furthermore, 15-HETE, produced from the same precursor as LXB4, was also significantly elevated by MWCNTs (Figure 5(E)). In contrast, 12-HETE was detected in both vehicle- and MWCNT-exposed lungs, but the means did not differ significantly (Figure 5(F)).

Induced production of SPMs from DHA

The lipidomics analysis also assessed the production of SPMs from docosahexaenoic acid. The pathways and major metabolites of SPMs from DHA were shown in Figure 6(A). DHA levels were detected at high levels in mouse lungs, with MWCNT exposure leading to an increase that did not reach statistical significance (Figure 6(B)). Notably, three resolvins (RvD2, RvD3, and RvD5) were found at picogram levels (Figures 6(C–E)), with RvD5 showing a statistically significant increase in MWCNT-exposed lungs compared to controls. Additionally, protectin D1 (PD1), protectin DX (PDX), and 17-hydroxydocosahexaenoic acid (HDHA), all produced from the same precursor as the RvDs, were elevated by MWCNTs, with the increases for PDX and 17-HDHA reaching statistical significance (Figures 6(F–H)). Maresins (MaRs), including MaR1 and 14S-HDHA, which are produced from 14S-hydroperoxydocosahexaenoic acid (HPDHA) via the Alox12-dependent pathway, were also significantly increased by MWCNT exposure (Figures 6(I and J)).

Induced production of SPMs from EPA

The pathways and enzymes involved in the production of resolvin Es and lipoxins from eicosapentaenoic acid were examined (Figure 7(A)). EPA levels were detected at high levels in vehicle-exposed lungs, with MWCNT exposure leading to an increase that did not reach statistical significance (Figure 7(B)). However, both RvE2 and 18-hydroxyeicosapentaenoic acid (HEPE) were significantly increased by MWCNTs (Figures 7(C and D)). Additionally, RvE4 and 15-HEPE, produced by Alox15 and Alox5, were detected and showed increases in MWCNT-exposed lungs, with the increase for 15-HEPE reaching a statistical significance (Figures 7(E and F)). Lastly, both 5-HEPE and 12-HEPE were detected and increased by MWCNTs, although these increases did not reach a statistical significance (Figures 7(G and H)).

Discussion

In this study, we demonstrated that pulmonary exposure to fibrogenic multiwalled carbon nanotubes stimulates the synthesis of both inflammatory lipid mediators and specialized pro-resolving mediators in mouse lungs at 7-days post-exposure. Our findings highlight the complex interplay between inflammation and resolution mechanisms in response to inhaled nanoparticles, providing insights into the temporal dynamics of lipid mediator production during the transition from acute inflammation to resolution.

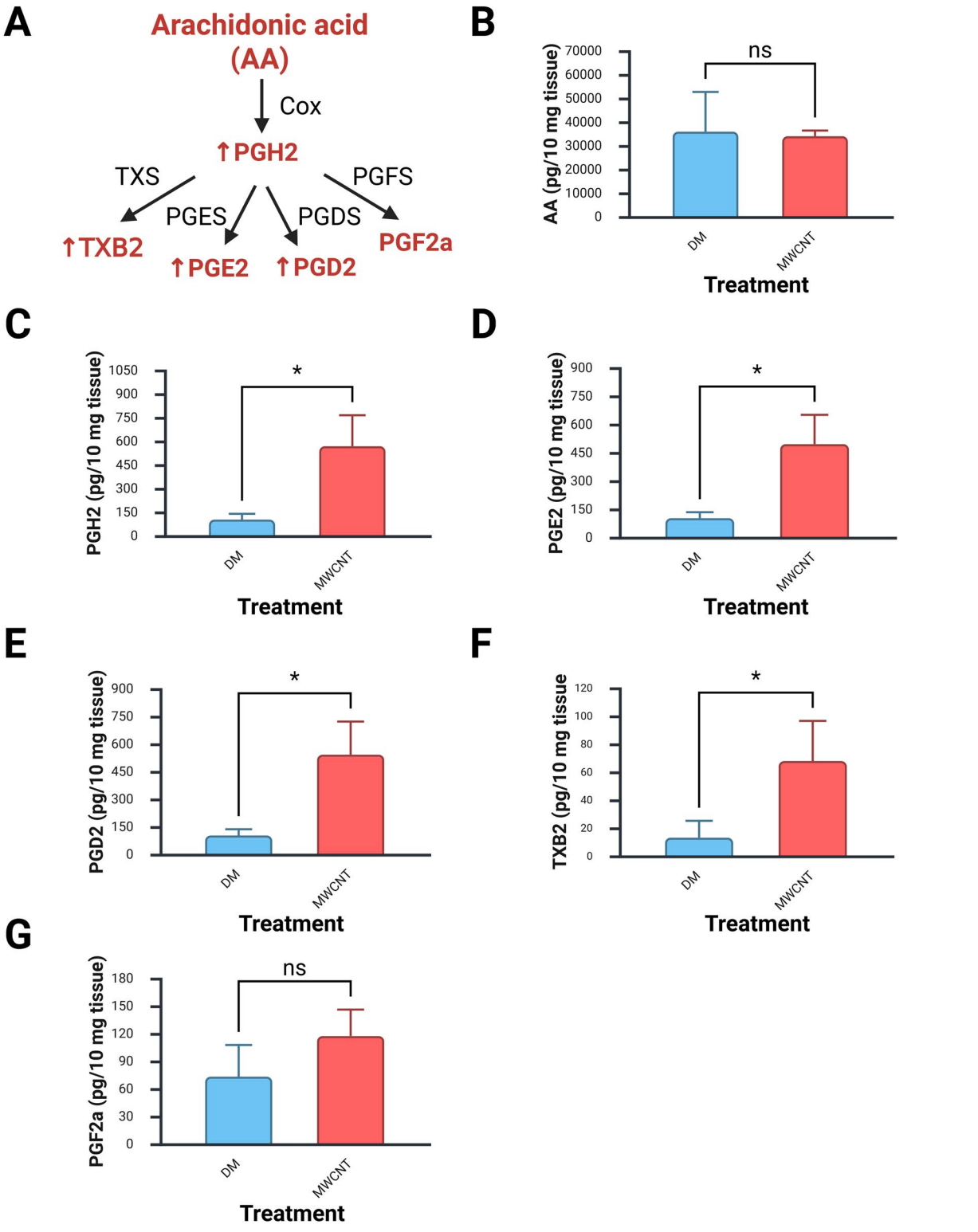

Figure 4. Induced production of PGs and TXs from arachidonic acid. Lung homogenates from mice treated with either vehicle or MWCNTs were analyzed by UPLC-MS/MS to quantify lipid mediators from the pathways of PG and TX synthesis. (A) Illustration of the production of ILMs through COX-mediated synthesis of PGs and TX from AA. Upward arrows indicate significantly increased lipid mediators. (B-G) Quantification of lipid mediator levels, including AA (B), PGH2 (C), PGE2 (D), PGD2 (E), TXB2 (F), and PGF2α (G). Data represent mean ± SD from samples of four mice in each group. Statistical significance is indicated as ns (non-significance) and $*p < 0.05$. Cox, cyclooxygenase; PGDS, prostaglandin D synthase; PGES, prostaglandin E synthase; PGFS, prostaglanding F synthase; and TXS, thromboxane synthase.

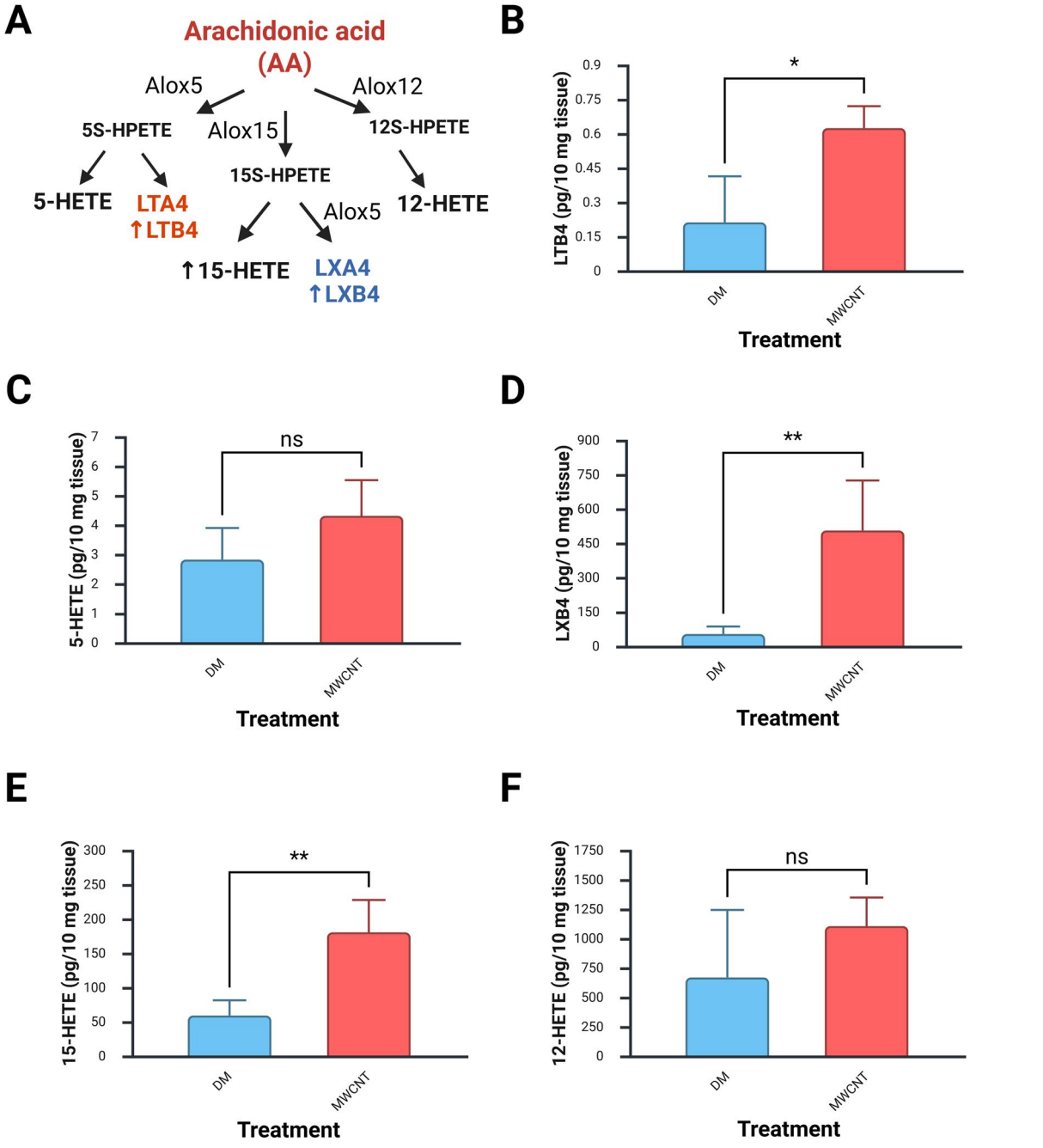

Figure 5. Induced production of LTs and LXs from arachidonic acid. Lung homogenates from mice treated with either vehicle or MWCNTs were analyzed by UPLC-MS/MS to quantify lipid mediators from the pathways of leukotriene and lipoxin synthesis. (A) Illustration of the production of LMs through Alox-mediated synthesis of LTs and LXs from AA. Upward arrows indicate significantly increased lipid mediators. (B-F) Quantification of lipid mediator levels, including LTB4 (B), 5-HETE (C), LXB4 (D), 15-HETE (E), and 12-HETE (F). Data represent mean ± SD from samples of four mice in each group. Statistical significance is indicated as ns (non-significance) and $*p < 0.05$; $**p < 0.01$. Alox, arachidonate lipoxygenase.

The acute inflammatory response observed at 1-day post-exposure to MWCNTs is characterized by significant neutrophil infiltration and the activation of proinflammatory pathways, including the rapid synthesis of ILMs such as prostaglandins and leukotrienes. This initial phase is critical for the clearance of inhaled particles; however, it can also lead to tissue damage if not resolved in a timely manner (Dong and Ma 2015). The subsequent transition to a macrophage-predominant response at 7-days post-exposure indicates a shift toward resolution, where M2 macrophages play a pivotal role in mediating tissue repair and the clearance of apoptotic cells and debris (Ma 2020).

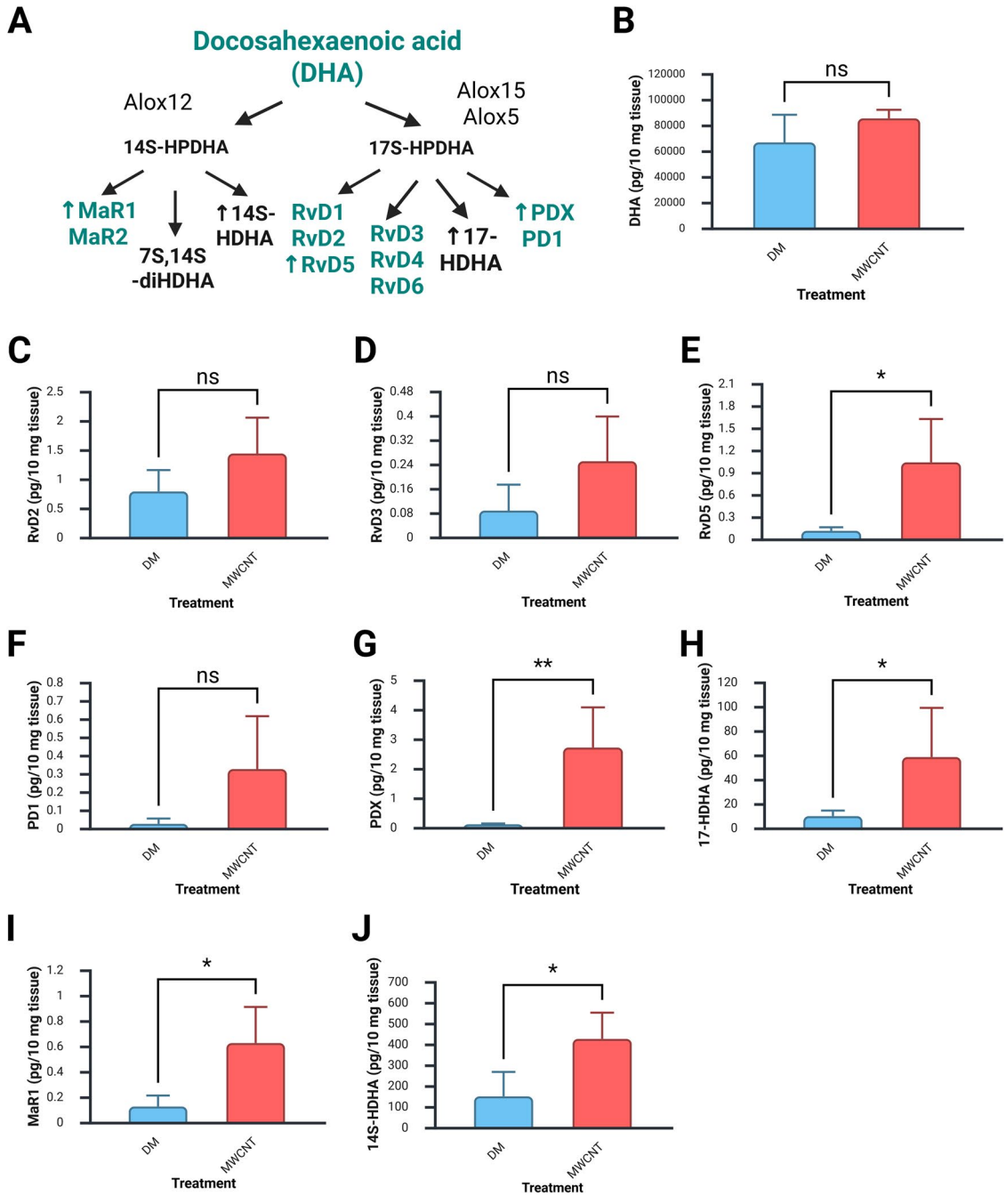

Figure 6. Induced production of SPMs from DHA. Lung homogenates from mice treated with either vehicle or MWCNTs were analyzed by UPLC-MS/MS to quantify lipid mediators from the pathways of SPM synthesis from DHA. (A) Illustration of the production of SPMs (RvDs, MaRs, and PDs) from DHA. Upward arrows indicate significantly increased lipid mediators. (B-J) Quantification of SPM levels, including DHA (B), RvD2 (C), RvD3 (D), RvD5 (E), PD1 (F), PDX (G), 17-HDHA (H), MaR1 (I), and 14S-HDHA (J). Data represent mean ± SD from samples of four mice in each group. Statistical significance is indicated as ns (non-significance) and *$p < 0.05$; **$p < 0.01$. Alox, arachidonate lipoxygenase.

Our lipidomics analysis revealed that MWCNTs significantly increased the production of both ILMs and SPMs at 7-days post-exposure. Among the LMs elevated, PGE2, PGD2, and LTB4 derived from arachidonic acid are potent ILMs that play critical roles in the initiation and amplification of acute inflammation. These ILMs promote inflammatory vascular and broncho responses and the chemotaxis and activation of various leukocytes, particularly, neutrophils and M1 macrophages, at or near the site of inflammation. Elevation of TXB2 signifies increased aggregation and activation of platelets that further increase inflammatory blood and vascular responses in acute inflammation. On the other hand, LXB4, derived from AA; RvD5, PDX, and MaR1 derived from DHA; and RvE2 derived from EPA, are potent SPMs elevated in mouse lungs by

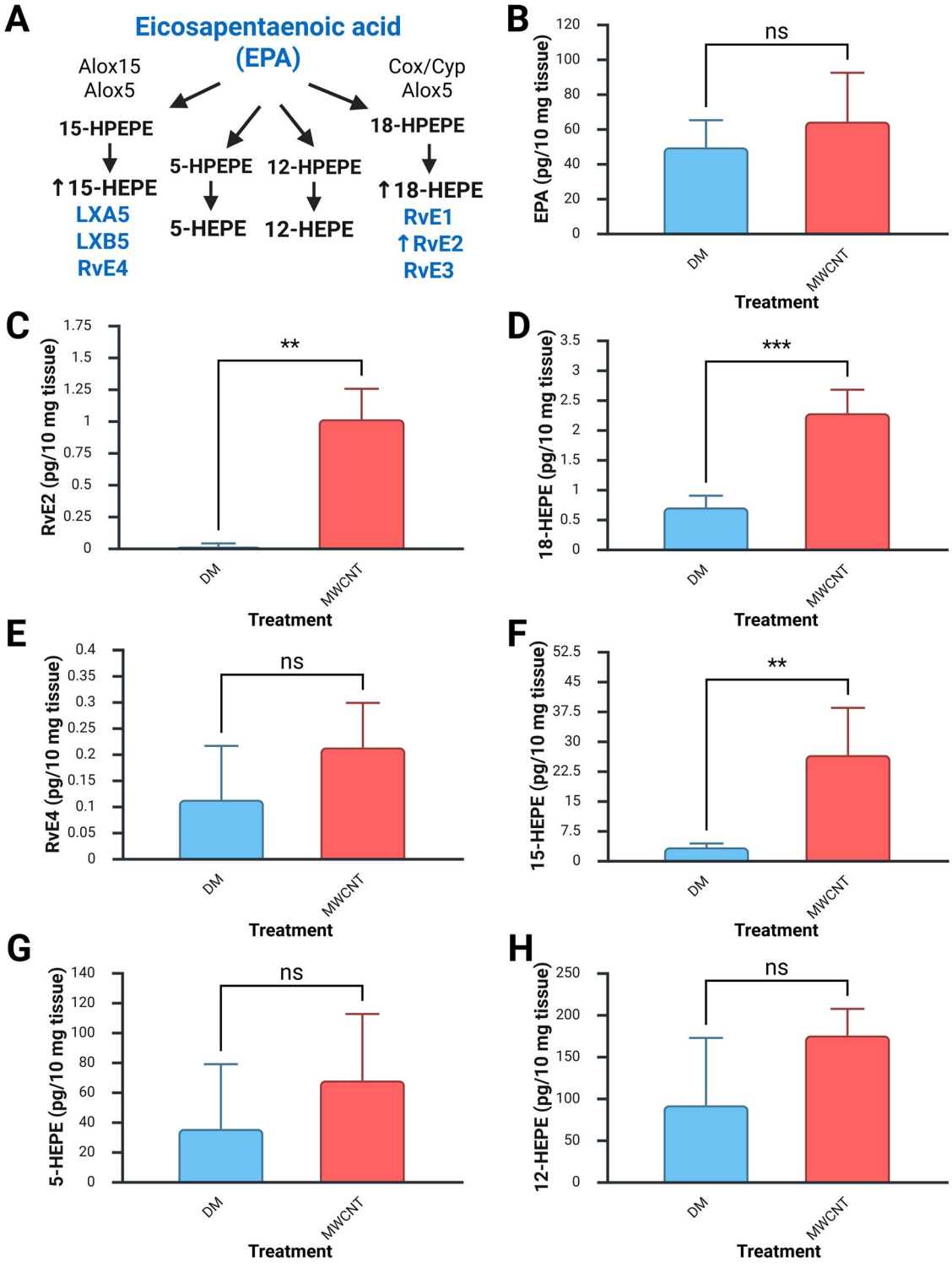

Figure 7. Induced production of SPMs from EPA. Lung homogenates from mice treated with either vehicle or MWCNTs were analyzed by UPLC-MS/MS to quantify lipid mediators from the pathways of SPM synthesis from EPA. (A) Illustration of the production of SPMs (RvEs and LXs) from EPA. Upward arrows indicate significantly increased lipid mediators. (B-H) Quantification of SPM levels, including EPA (B), RvE2 (C), 18-HEPE (D), RvE4 (E), 15-HEPE (F), 5-HEPE (G), and 12-HEPE (H). Data represent mean ± SD from samples of four mice in each group. Statistical significance is indicated as ns (non-significance) and $^{**}p < 0.01$; $^{***}p < 0.001$. Alox, arachidonate lipoxygenase; Cox, cyclooxygenase; Cyp, cytochrome P-450.

MWCNTs. Among the SPMs, LXB4 potently inhibits leukocyte recruitment to dampen and resolve inflammation, whereas the resolvins boost resolution responses by promoting type 2 inflammation while inhibiting type 1 inflammation through regulating the polarization of immune cells (Serhan, Chiang, and Dalli 2015).

Therefore, MWCNTs stimulate the production of a signature of ILMs and SPMs to provoke an inflammatory response that continues the clearance of deposited nanoparticles and, at the same time, initiates mechanisms aimed at resolving inflammation to limit tissue damage, promote tissue repair, and maintain pulmonary homeostasis.

The observed accumulation of phospholipids in macrophages following MWCNT exposure further supports the notion that macrophages are actively engaged in lipid mediator biosynthesis. Phospholipids can serve as precursors for the synthesis of both ILMs and SPMs, and their increased levels in macrophages may reflect enhanced membrane remodeling and the activation of lipid metabolic pathways. This finding aligns with previous studies indicating that macrophages can modulate their lipid profiles in response to environmental stimuli, thereby influencing the local inflammatory milieu (Lim et al. 2020, Ma 2020, Ma et al. 2025).

The biphasic nature of the inflammatory response to MWCNTs, characterized by an initial neutrophilic phase followed by an M2 macrophage-dominated phase, mirrors the dynamics observed in other models of inflammation in the lung and other organs (Wynn and Ramalingam 2012). This biphasic response is essential for effective resolution, as it allows for the timely clearance of inflammatory cells and the restoration of tissue homeostasis. The transition from type 1 to type 2 inflammation, as evidenced by the shift from neutrophil to macrophage predominance, is a critical determinant of whether the inflammatory response resolves appropriately or progresses to chronic inflammation and fibrosis (Serhan, Chiang, and Van Dyke 2008). If and how lipid mediators directly impact fibrotic progression remain unclear and warrant further investigation.

The findings of this study have significant implications for understanding the health risks associated with exposure to nanomaterials and other respirable particles. Given the potential for MWCNTs to induce both acute and chronic inflammatory responses, it is crucial to further investigate the mechanisms underlying these effects and their long-term consequences on lung health. Future studies should explore the signaling pathways involved in the production of ILMs and SPMs in response to MWCNTs, as well as the potential for therapeutic interventions targeting these pathways to mitigate the adverse effects of nanomaterial exposure.

In conclusion, our study provides new insights into the role of lipid mediators in the inflammatory response to MWCNTs, highlighting the importance of both ILMs and SPMs in the transition from inflammation to resolution. Understanding these mechanisms may inform the development of strategies to prevent or treat lung diseases associated with exposure to inhaled nanoparticles.

Acknowledgement

The findings and conclusions in this report are those of the authors and do not necessarily represent the official position of the National Institute for Occupational Safety and Health, Centers for Disease Control and Prevention.

Mention of any company or product does not constitute endorsement by the National Institute for Occupational Safety and Health, Centers for Disease Control and Prevention.

Author contributions

Q.M. and R.F.L conceived the study; Q.M., C.S.L., R.F.L., C.C.R., and J.H.P. designed the study, provided reagents, and performed experiments; Q.M. and C.S.L. performed data analysis and statistical analysis; Q.M. wrote the manuscript. All authors contributed to manuscript preparation and finalization.

Disclosure statement

No potential conflict of interest was reported by the authors.

Funding

This work was funded by the Nanotechnology Research Center program under Grant 9390P0G (Q.M.) at the National Institute for Occupational Safety and Health, Centers for Disease Control and Prevention, USA.

Data availability statement

The authors confirm that the data supporting the findings of this study are available within the article and its supplementary materials.

References

Chiang, N., and C. N. Serhan. 2020. "Specialized Pro-Resolving Mediator Network: An Update on Production and Actions." *Essays in Biochemistry* 64 (3): 443–462. https://doi.org/10.1042/EBC20200018.

De Volder, M. F., S. H. Tawfick, R. H. Baughman, and A. J. Hart. 2013. "Carbon Nanotubes: present and Future Commercial Applications." *Science (New York, N.Y.)* 339 (6119): 535–539. https://doi.org/10.1126/science.1222453.

Donaldson, K., R. Aitken, L. Tran, V. Stone, R. Duffin, G. Forrest, and A. Alexander. 2006. "Carbon Nanotubes: A Review of Their Properties in Relation to Pulmonary Toxicology and Workplace Safety." *Toxicological Sciences: An Official Journal of the Society of Toxicology* 92 (1): 5–22. https://doi.org/10.1093/toxsci/kfj130.

Dong, J., and Q. Ma. 2015. "Advances in Mechanisms and Signaling Pathways of Carbon Nanotube Toxicity."

Nanotoxicology 9 (5): 658–676. https://doi.org/10.3109/17435390.2015.1009187.

Dong, J., and Q. Ma. 2016. "In Vivo Activation of a T Helper 2-Driven Innate Immune Response in Lung Fibrosis Induced by Multi-Walled Carbon Nanotubes." *Archives of Toxicology* 90 (9): 2231–2248. https://doi.org/10.1007/s00204-016-1711-1.

Dong, J., and Q. Ma. 2018b. "Macrophage Polarization and Activation at the Interface of Multi-Walled Carbon Nanotube-Induced Pulmonary Inflammation and Fibrosis." *Nanotoxicology* 12 (2): 153–168. https://doi.org/10.1080/17435390.2018.1425501.

Dong, J., and Q. Ma. 2018a. "Type 2 Immune Mechanisms in Carbon Nanotube-Induced Lung Fibrosis." *Frontiers in Immunology* 9: 1120. https://doi.org/10.3389/fimmu.2018.01120.

Dong, J., and Q. Ma. 2019. "Integration of Inflammation, Fibrosis, and Cancer Induced by Carbon Nanotubes." *Nanotoxicology* 13 (9): 1244–1274. https://doi.org/10.1080/17435390.2019.1651920.

Dong, J., D. W. Porter, L. A. Batteli, M. G. Wolfarth, D. L. Richardson, and Q. Ma. 2015. "Pathologic and Molecular Profiling of Rapid-Onset Fibrosis and Inflammation Induced by Multi-Walled Carbon Nanotubes." *Archives of Toxicology* 89 (4): 621–633. https://doi.org/10.1007/s00204-014-1428-y.

Erdely, A., M. Dahm, B. T. Chen, P. C. Zeidler-Erdely, J. E. Fernback, M. E. Birch, D. E. Evans, et al. 2013. "Carbon Nanotube Dosimetry: From Workplace Exposure Assessment to Inhalation Toxicology." *Particle and Fibre Toxicology* 10 (1): 53. https://doi.org/10.1186/1743-8977-10-53.

Galer, D. M., H. W. Leung, R. G. Sussman, and R. J. Trzos. 1992. "Scientific and Practical Considerations for the Development of Occupational Exposure Limits (OELs) for Chemical Substances." *Regulatory Toxicology and Pharmacology: RTP* 15 (3): 291–306. https://doi.org/10.1016/0273-2300(92)90040-g.

Hughes, K. J., J. Cheng, K. A. Iyer, K. Ralhan, M. Ganesan, C. W. Hsu, Y. Zhan, et al. 2024. "Unveiling Trends: Nanoscale Materials Shaping Emerging Biomedical Applications." *ACS Nano* 18 (26): 16325–16342. https://doi.org/10.1021/acsnano.4c04514.

Lim, C. S., B. Veltri, M. Kashon, D. W. Porter, and Q. Ma. 2023. "Multi-Walled Carbon Nanotubes Induce Arachidonate 5-Lipoxygenase Expression and Enhance the Polarization and Function of M1 Macrophages In Vitro." *Nanotoxicology* 17 (3): 249–269. https://doi.org/10.1080/17435390.2023.2204161.

Lim, C. S., D. W. Porter, M. S. Orandle, B. J. Green, M. A. Barnes, T. L. Croston, M. G. Wolfarth, et al. 2020. "Resolution of Pulmonary Inflammation Induced by Carbon Nanotubes and Fullerenes in Mice: Role of Macrophage Polarization." *Frontiers in Immunology* 11: 1186. https://doi.org/10.3389/fimmu.2020.01186.

Lim, C. S., J. K. Gu, and Q. Ma. 2025. "The ETS Domain-Containing Hematopoietic Transcription Factor PU.1 Mediates the Induction of Arachidonate 5-Lipoxygenase by Multi-Walled Carbon Nanotubes in Macrophages In Vitro." *Archives of Toxicology* 99 (2): 597–610. https://doi.org/10.1007/s00204-024-03925-w.

Ma, Q. 2020. "Polarization of Immune Cells in the Pathologic Response to Inhaled Particulates." *Frontiers in Immunology* 11: 1060. https://doi.org/10.3389/fimmu.2020.01060.

Ma, Q., R. F. LeBouf, C. Rimayi, C. S. Lim, D. Fekedulegn, J. H. Park, and D. W. Porter. 2025. "Sterile inflammation in mouse lung driven by lipid mediator pathways following MWCNT exposure." Chemical Research in Toxicology, Articles ASAP, Publication Date (Web): December 15, 2025. https://doi.org/10.1021/acs.chemrestox.5c00470.

Mercer, R. R., J. F. Scabilloni, A. F. Hubbs, L. A. Battelli, W. McKinney, S. Friend, M. G. Wolfarth, M. Andrew, V. Castranova, and D. W. Porter. 2013. "Distribution and Fibrotic Response following Inhalation Exposure to Multi-Walled Carbon Nanotubes." *Particle and Fibre Toxicology* 10 (1): 33. https://doi.org/10.1186/1743-8977-10-33.

NIOSH. 2013. Occupational exposure to carbon nanotubes and nanofibers. Cincinnati, OH: U.S. Department of Health and Human Services, Centers for Disease Control and Prevention, National Institute for Occupational Safety and Health, DHHS (NIOSH). Publication No. 2013-145. https://www.cdc.gov/niosh/docs/2013-145."

Phalen, R. F. 2008. *The Respiratory Tract. Inhalation Studies: Foundations and Techniques. R. F. Phalen.* Boca Raton, CRC Press, 33–68.

Porter, D. W., A. F. Hubbs, R. R. Mercer, N. Wu, M. G. Wolfarth, K. Sriram, S. Leonard, et al. 2010. "Mouse Pulmonary Dose- and Time Course-Responses Induced by Exposure to Multi-Walled Carbon Nanotubes." *Toxicology* 269 (2–3): 136–147. https://doi.org/10.1016/j.tox.2009.10.017.

Rao, G. V., S. Tinkle, D. N. Weissman, J. M. Antonini, M. L. Kashon, R. Salmen, L. A. Battelli, P. A. Willard, M. D. Hoover, and A. F. Hubbs. 2003. "Efficacy of a Technique for Exposing the Mouse Lung to Particles Aspirated from the Pharynx." *Journal of Toxicology and Environmental Health. Part A* 66 (15): 1441–1452. https://doi.org/10.1080/15287390306417.

Ricciotti, E., and G. A. FitzGerald. 2011. "Prostaglandins and Inflammation." *Arteriosclerosis, Thrombosis, and Vascular Biology* 31 (5): 986–1000. https://doi.org/10.1161/ATVBAHA.110.207449.

Sayers, B. C., A. J. Taylor, E. E. Glista-Baker, J. K. Shipley-Phillips, R. T. Dackor, M. L. Edin, F. B. Lih, et al. 2013. "Role of Cyclooxygenase-2 in Exacerbation of Allergen-Induced Airway Remodeling by Multiwalled Carbon Nanotubes." *American Journal of Respiratory Cell and Molecular Biology* 49 (4): 525–535. https://doi.org/10.1165/rcmb.2013-0019OC.

Serhan, C. N., and J. Savill. 2005. "Resolution of Inflammation: The Beginning Programs the End." *Nature Immunology* 6 (12): 1191–1197. https://doi.org/10.1038/ni1276.

Serhan, C. N., N. Chiang, and J. Dalli. 2015. "The Resolution Code of Acute Inflammation: Novel Pro-Resolving Lipid Mediators in Resolution." *Seminars in Immunology* 27 (3): 200–215. https://doi.org/10.1016/j.smim.2015.03.004.

Serhan, C. N., N. Chiang, and T. E. Van Dyke. 2008. "Resolving Inflammation: dual anti-Inflammatory and Pro-Resolution Lipid Mediators." *Nature Reviews. Immunology* 8 (5): 349–361. https://doi.org/10.1038/nri2294.

Sinnott, S. B., and R. Andrews. 2001. "Carbon Nanotubes: Synthesis, Properties, and Applications." *Critical Reviews in Solid State and Materials Sciences* 26 (3): 145–249. https://doi.org/10.1080/20014091104189.

Stone, K. C., R. R. Mercer, P. Gehr, B. Stockstill, and J. D. Crapo. 1992. "Allometric Relationships of Cell Numbers and Size in the Mammalian Lung." *American Journal of Respiratory Cell and Molecular Biology* 6 (2): 235–243. https://doi.org/10.1165/ajrcmb/6.2.235.

Suzui, M., M. Futakuchi, K. Fukamachi, T. Numano, M. Abdelgied, S. Takahashi, M. Ohnishi, et al. 2016. "Multiwalled Carbon Nanotubes Intratracheally Instilled into the

Rat Lung Induce Development of Pleural Malignant Mesothelioma and Lung Tumors." *Cancer Science* 107 (7): 924–935. https://doi.org/10.1111/cas.12954.

Wynn, T. A., and T. R. Ramalingam. 2012. "Mechanisms of Fibrosis: Therapeutic Translation for Fibrotic Disease." *Nature Medicine* 18 (7): 1028–1040. https://doi.org/10.1038/nm.2807.

Zhang, Q., J. Q. Huang, W. Z. Qian, Y. Y. Zhang, and F. Wei. 2013. "The Road for Nanomaterials Industry: A Review of Carbon Nanotube Production, Post-Treatment, and Bulk Applications for Composites and Energy Storage." *Small (Weinheim an Der Bergstrasse, Germany)* 9 (8): 1237–1265. https://doi.org/10.1002/smll.201203252.